

## Electronic Supplementary Information: Atomic-Scale Detection of Individual Lead Clusters Confined in Linde Type A Zeolites

Jarmo Fatermans<sup>†a,b</sup>, Giacomo Romolini<sup>‡d</sup>, Thomas Altantzis<sup>†a,b,c</sup>, Johan Hofkens<sup>d,e</sup>, Maarten B. J. Roeffaers<sup>\*f</sup>, Sara Bals<sup>a,b</sup>, and Sandra Van Aert<sup>\*a,b</sup>

<sup>a</sup> Electron Microscopy for Materials Science (EMAT), University of Antwerp, Groenenborgerlaan 171, 2020 Antwerp, Belgium. E-mail: sandra.vanaert@uantwerpen.be

<sup>b</sup> NANOLab Center of Excellence, University of Antwerp, Belgium. E-mail: sandra.vanaert@uantwerpen.be

<sup>c</sup> Applied Electrochemistry and Catalysis Group (ELCAT), University of Antwerp, Universiteitsplein 1, 2610 Wilrijk, Belgium.

<sup>d</sup> Molecular Imaging and Photonics, Department of Chemistry, KU Leuven, Celestijnenlaan 200F, 3001 Leuven, Belgium.

<sup>e</sup> Max Planck Institute for Polymer Research, Ackermannweg 10, 55128 Mainz, Germany.

<sup>f</sup> Centre for Membrane Separations, Adsorption, Catalysis, And Spectroscopy for Sustainable Solutions (cMACS), KU Leuven, Celestijnenlaan 200F, Box 2461, 3001, Leuven, Belgium. E-mail: maarten.roeffaers@kuleuven.be

‡ These authors contributed equally to this work.

### S1 Photoluminescence characterization

The incorporation of Pb atoms in the Linde Type A (LTA) zeolite samples was verified via photoluminescence spectroscopy which revealed a bright purple photoluminescence with a maximum emission at 390 nm (see Figure S1). This luminescence is related to Pb<sub>4</sub> clusters, as determined in recent work through a combination of extended X-ray absorption fine structure (EXAFS) and optical spectroscopy.<sup>1</sup> For the luminescence measurements, the heat-treated Pb-LTA samples were placed into a quartz cuvette (1 mm optical path). Emission and excitation spectra were recorded using an Edinburgh FLS980 fluorimeter, operated in front-face mode.

### S2 Template matching

For improving the perceived quality of an acquired raw HAADF STEM image, an arbitrary section of the image, centered around a projected SOD cage, has been selected to serve as a template. Then, a template-matching routine was used to find similar regions within the image. The similarity between the chosen template and other sections of the image was evaluated by the sum of absolute differences (SAD).<sup>2</sup> As such, regions of the image that show enough similarity with the original template, according to a threshold value, could be extracted and summed, or, equivalently, averaged in order to obtain a representation of the raw HAADF STEM image with better SNR and CNR. This is illustrated in Figure 1, where the chosen template has been matched with 334, 922, and 946 regions for Figure 1(a), (b), and (c), respectively. Interestingly, the HAADF STEM imaging mode exhibits a strong

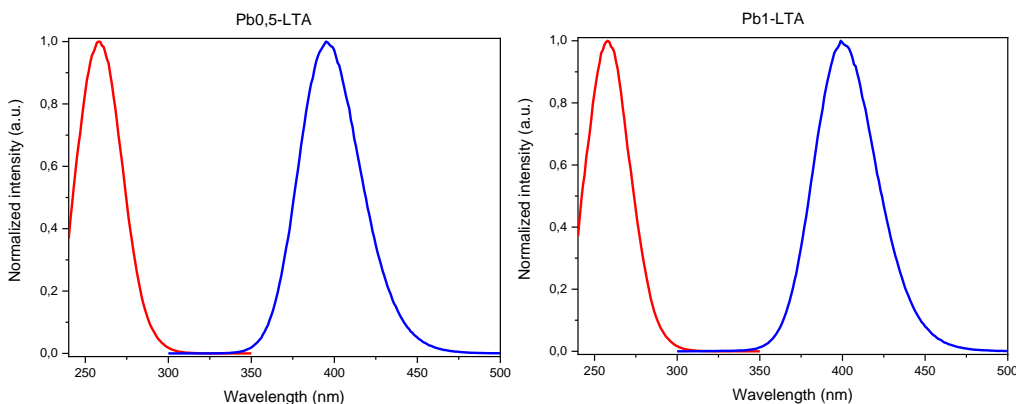


**Figure S1.** Emission (blue curves) and excitation (red curves) spectra of a Pb<sub>0.5</sub>-LTA zeolite (left) and Pb<sub>1</sub>-LTA zeolite (right). Emission spectra recorded with  $\lambda_{exc} = 255$  nm and excitation spectra recorded with  $\lambda_{ems} = 395$  nm.

dependence on the atomic number.<sup>3,4</sup> As a result, heavier atoms are displayed brighter as compared to lighter ones in HAADF STEM. As such, in Figure 1, it can be assumed that locations of projected Pb atomic columns will appear with higher intensity than positions related to the elements of the zeolite framework, i.e. Si, Al, and O. By comparing the insets of Figure 1, it is clear that the amount of Pb within the SOD cages is different in the imaged samples because of the varying intensity of the projected Pb atomic columns as compared to the zeolite framework. For the over-exchanged Pb-LTA zeolite in Figure 1(a), the amount of Pb, incorporated within the SOD cages of the zeolite, is so high that it dominates the surrounding observed atomic column intensities. Therefore, the intensities related to Si, Al, and O of the zeolite framework cannot directly be observed. In Figure 1(b), though, a lower amount of Pb as compared to Figure 1(a) is present within the SOD cages. In this case, the bright spots related to Pb atomic columns are still present, but they are not dominating the intensities of the other atom types to such an extent as in Figure 1(a). As such, for the Pb<sub>1</sub>-LTA zeolite shown in Figure 1(b), the intensities corresponding to the zeolite elements are visible. Lastly, for the Pb<sub>0.5</sub>-LTA zeolite in Figure 1(c), the concentration of Pb within the SOD cages is even lower than in Figure 1(b). This causes the Pb atomic column intensities to decrease even further and, in this case, it is even the zeolite framework that dominates the averaged template-matching image given by the inset of Figure 1(c). Directly comparing the observed intensities in the insets of Figure 1 provides already some qualitative insight into the amount of Pb present within the SOD cages. It is noted, though, that these template-matched images only provide averaged information on the Pb concentration in the sample, losing information at the local scale. Especially from Figure 1(b) for example, it can be seen that there are local intensity variations throughout the image, corresponding to local variations of the number of Pb atoms in the SOD cages, which cannot be captured by template-matched images.

### S3 Powder XRD measurements

In Table S1, the occupancy factors (following from X-ray diffraction (XRD) analysis which measure the fraction of molecules occupying a specific position in a crystal) of all Pb positions within an over-exchanged Pb-LTA zeolite are mentioned. It stands out that the occupancy of the Pb-4 position is significantly lower, and almost negligible, as compared to the occupancies of the other Pb positions. As such, it is expected that the observed intensities from Pb-4 positions in HAADF STEM data of an over-exchanged Pb-LTA zeolite should be considerably lower than the ones related to other Pb positions. This is confirmed from Figure S2(a), and, especially, from Figure S2(b), showing the corresponding template-matching image, superimposed with the estimated positions derived from XRD measurements. From these figures, no significant intensities are observed at the Pb-4 locations, in correspondence with the very low occupancy reported in Table S1. In general, based on the average HAADF STEM image of Figure S2(b), a reasonable agreement is found between the STEM data and the positions and occupancy factors obtained by XRD analysis. The combined intensities related to the Pb-1 and Pb-3 positions dominate, because of their close projected distance when viewed along the [100] zone axis. Similar figures as Figures S2(a) and (b) have also been displayed for the Pb<sub>1</sub>-LTA zeolite and the Pb<sub>0.5</sub>-LTA zeolite in Figures S2(c) and (d), and Figures S2(e) and (f), respectively. Also here, a good agreement is found between the HAADF STEM image data and the estimated Pb positions from XRD analysis. Furthermore, due to the reduced Pb concentration in these images, also the alignment of the STEM data with the estimated positions of the zeolite framework elements can be observed.

Pb atom positions	Occupancy
Pb-1	0.214
Pb-2	0.167
Pb-3	0.435
Pb-4	0.025

**Table S1.** Occupancy factors of the different Pb positions within an over-exchanged Pb-LTA zeolite obtained by XRD analysis.

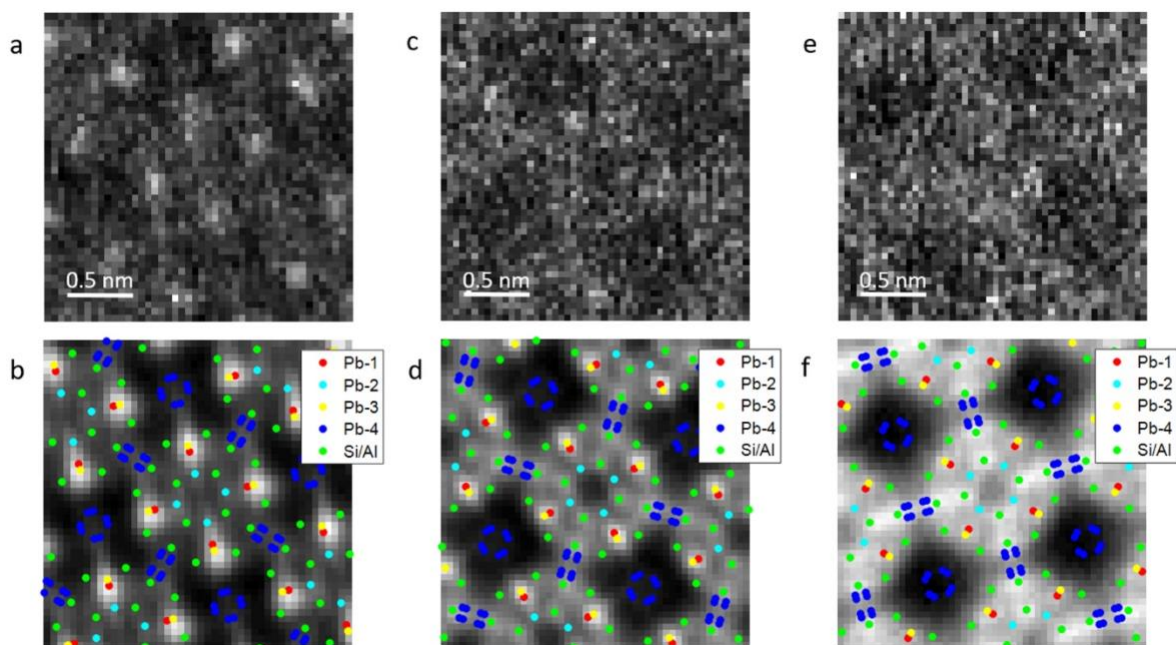


**Figure S2.** (a), (c), and (e) Enlarged regions of the high-resolution HAADF STEM images of over-exchanged Pb-LTA, Pb<sub>1</sub>-LTA, and Pb<sub>0.5</sub>-LTA zeolites, respectively, shown in Figure 1. (b), (d), and (f) Corresponding averaged images by using template matching with 334, 1069, and 877 templates, respectively, overlain with the estimated coordinates from XRD analysis, shown as colored dots, of the elements displayed in the legends. For clarity, closely located coordinates have been merged, no explicit distinction is made between coordinates related to the Si and Al positions of the zeolite framework, and coordinates related to O positions have not been displayed.

#### S4 TEM image simulation

A complete list of simulation parameters is displayed in Table S2.

Parameter	Symbol	Value
Acceleration voltage	$V_0$ (kV)	300
Defocus	$\epsilon$ (Å)	2.3
Spherical aberration	$C_s$ (mm)	0.001
Spherical aberration of 5th order	$C_5$ (mm)	0
Semiconvergence angle	$\alpha$ (mrad)	21.3
Detector inner radius	$\beta_1$ (mrad)	35
Detector outer radius	$\beta_2$ (mrad)	190
Pixel size	$\Delta x = \Delta y$ (Å)	0.485

**Table S2.** Microscope parameter values for simulation of HAADF STEM images of a Pb-LTA zeolite using MULTTEM.

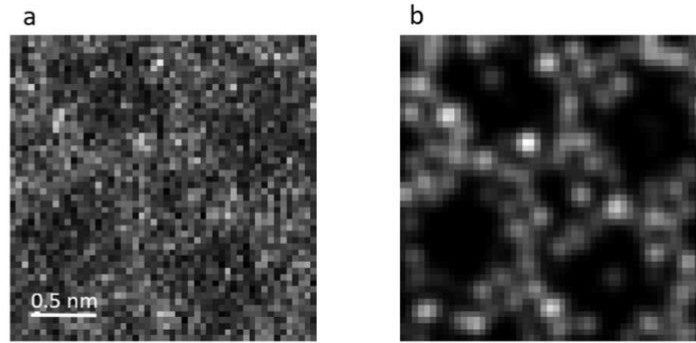


**Figure S3.** (a) Example of an individual template-matched region of the high-resolution HAADF STEM image data of the  $\text{Pb}_1$ -LTA zeolite sample viewed along the  $[100]$  zone axis. (b) Refined model of the experimental image data in (a). Despite the fact that (a) exhibits low SNR, the model-fitting routine still enables to extract relevant features from the acquired raw HAADF STEM image data.

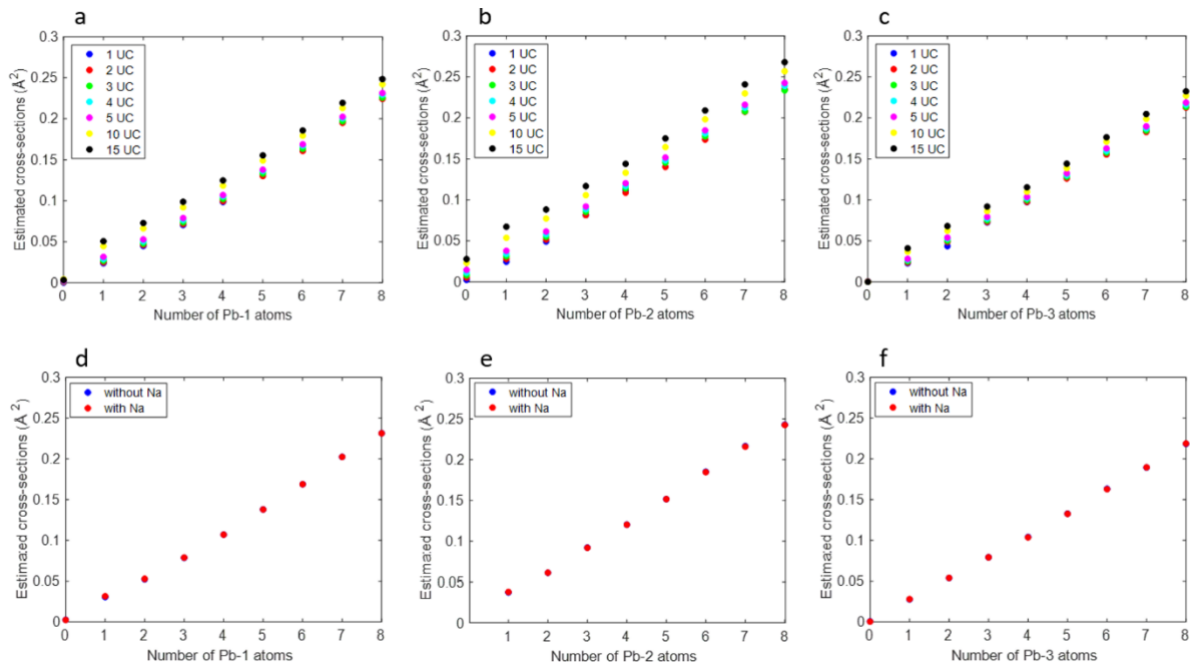


**Figure S4.** (a)-(c) Estimated cross-sections of a Pb-1, Pb-2, and Pb-3 column, respectively, from simulated HAADF STEM images as a function of number of Pb atoms for varying surrounding zeolite thicknesses expressed in terms of number of unit cells (UCs). It can be seen that the zeolite thickness influences the estimated cross-sections of the Pb atoms. Therefore, it is important to take thickness into consideration when comparing simulated Pb cross-sections to experimental ones in order to avoid miscounting of the number of Pb atoms as much as possible along a projected atomic column in the HAADF STEM image data. (d)-(f) Comparison of the estimated cross-sections of a Pb-1, Pb-2, and Pb-3 column, respectively, between taking the effect of Na atoms into consideration and neglecting Na atoms, for a zeolite thickness of 5 UC. It can be observed that the influence on the cross-sections of the Pb atoms of remaining Na atoms after Pb exchange is negligible. This is due to the fact that the number of Na atoms after incorporation of Pb atoms in the LTA zeolite is limited and because Na is much lighter as compared to Pb.

## S5 Parametric model fitting

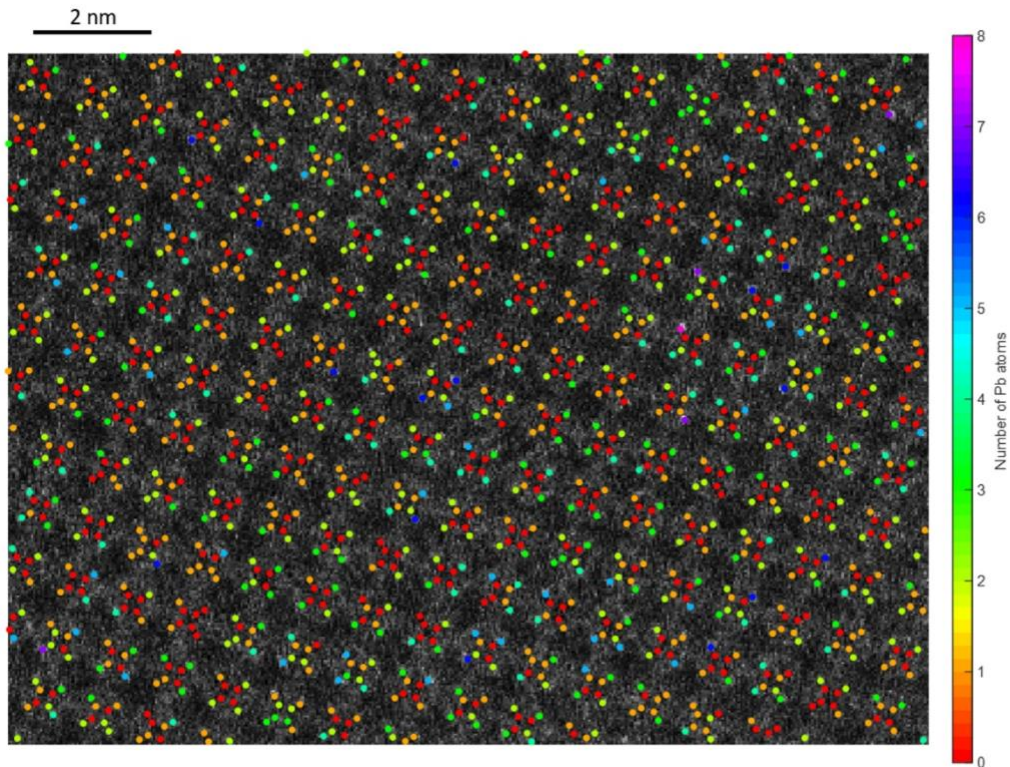


**Figure S5.** High-resolution HAADF STEM image of the Pb<sub>1</sub>-LTA zeolite sample acquired along the [100] zone axis, in correspondence to Figure 2(c), overlain with the estimated number of Pb atoms observed along the viewing direction of the SOD cages. For clarity, the atom-counting results of the closely located Pb-1 and Pb-3 positions in the image plane have been merged.

In Figure S3, an example of an optimized model is shown. It is noted that for stabilizing the fitting procedure, the atomic column positions have been fixed, in accordance to the positions derived from XRD analysis (see Figure S2).

## S6 Atom counting

Figures S4(a)-(c) show the cross sections calculated from image simulations of the different kinds of Pb columns as a function of the number of Pb atoms in the column. In the image simulations, also the effect of Na atoms has been taken into account, but it could be observed that their influence was negligible as compared to the much heavier Pb atoms (see Figures S4(d)-(f)). Figures S5 and S6 show more detailed representations of the atom-counting results shown in Figures 2(c) and (d), respectively.

## S7 Thickness estimation

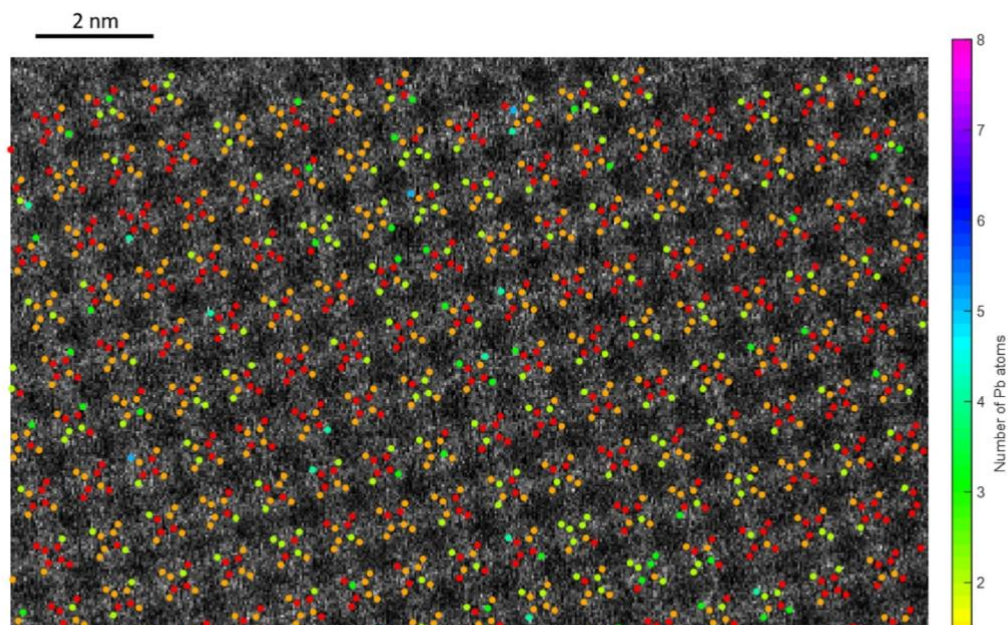


**Figure S6.** High-resolution HAADF STEM image of the  $\text{Pb}_{0.5}$ -LTA zeolite sample acquired along the [100] zone axis, in correspondence to Figure 2(d), overlain with the estimated number of Pb atoms observed along the viewing direction of the SOD cages. For clarity, the atom-counting results of the closely located Pb-1 and Pb-3 positions in the image plane have been merged.

For measuring the thickness of the  $\text{Pb}_1$ -LTA and  $\text{Pb}_{0.5}$ -LTA zeolite samples, the cross-sections of the projected Si/Al columns within the SOD cages (see Figure S2) have been measured by using the described model-fitting parameter-estimation procedure. Hereby, the experimentally determined cross-sections are compared with the cross-sections of the corresponding Si/Al columns obtained from simulated HAADF STEM images of a none Pb-loaded zeolite framework with varying thickness. In Figure S7(a), the

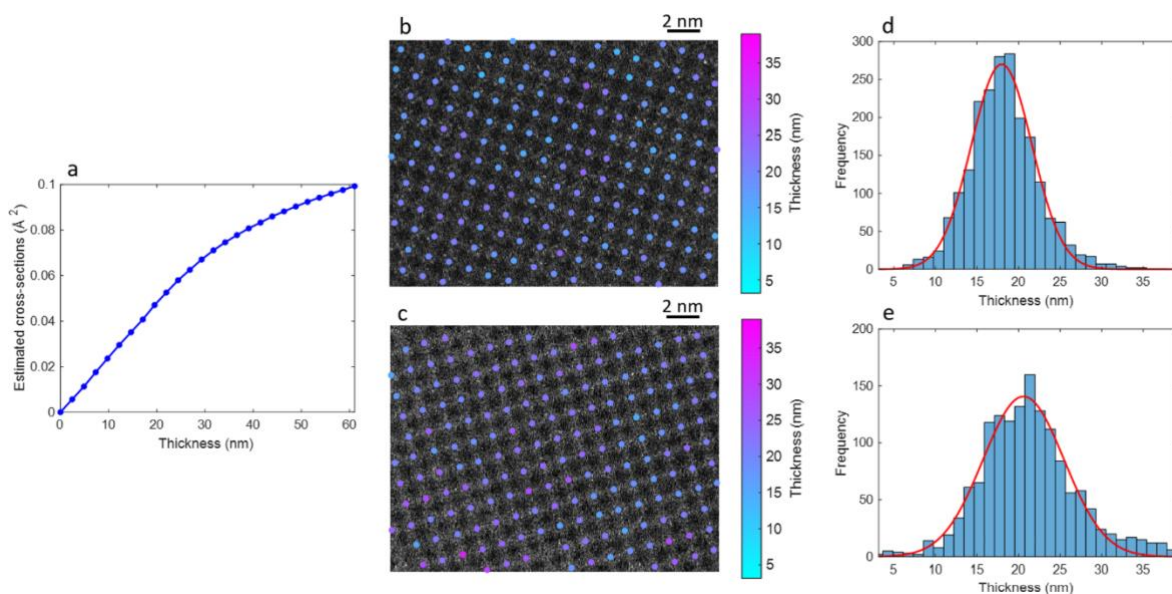


**Figure S7.** (a) Estimated cross-sections of a Si/Al column from simulated HAADF STEM images as a function of sample thickness. (b) and (c) Examples of high-resolution HAADF STEM image data, corresponding to Figures 1(b) and (c), of  $\text{Pb}_1$ -LTA and  $\text{Pb}_{0.5}$ -LTA zeolites, respectively, overlain with the estimated thickness values. (d) and (e) Thickness distributions of the  $\text{Pb}_1$ -LTA and  $\text{Pb}_{0.5}$ -LTA samples, respectively, ranging from 3.2 nm to 39.0 nm. The red curves correspond to normal distributions with mean  $\mu = 18$  nm and standard deviation  $\sigma = 4$  nm for (d), and  $\mu = 21$  nm and  $\sigma = 5$  nm for (e).

cross-sections of a simulated Si/Al column are shown as a function of thickness. As in Figure 2(b), a monotonically increasing relationship is observed. As a result, by comparing experimental cross-sections with simulated ones, Figure S7(a), allows for a direct correlation with sample thickness. Figures S7(b) and (c) show raw HAADF STEM images of the Pb<sub>1</sub>-LTA and Pb<sub>0.5</sub>-LTA samples, respectively, superimposed with an estimation of the thickness obtained by comparing the experimental and simulated cross-sections of the Si/Al columns. In Figures S7(d) and (e), histograms of the estimated thicknesses have been displayed of the Pb<sub>1</sub>-LTA and Pb<sub>0.5</sub>-LTA zeolite samples, respectively. From these histograms, the average thickness and standard deviation of both samples can be derived by describing the histograms by normal distributions. As such, the mean thickness of the Pb<sub>1</sub>-LTA zeolite sample is estimated to be  $18 \pm 4$  nm, whereas for Pb<sub>0.5</sub>-LTA the mean thickness equals  $21 \pm 5$  nm. From these measures, it can be concluded that the thickness distributions of the Pb<sub>1</sub>-LTA and Pb<sub>0.5</sub>-LTA samples are comparable, despite a slightly larger thickness estimate and variance for the Pb<sub>0.5</sub>-LTA zeolite. These results suggest that local intensity differences observed between the HAADF STEM image data of the Pb<sub>1</sub>-LTA zeolite and the Pb<sub>0.5</sub>-LTA zeolite are not related to thickness variations, but to a different concentration of Pb atoms within the SOD cages of the zeolites.

## S8 Atom counting and occupancy uncertainties

Uncertainties on atom counting results have been determined by calculating the variance of the corresponding cross-sections. Scattering cross-sections are robust to many imaging parameters, in particular those that control probe size, such as, defocus and spherical aberration.<sup>5,6</sup> The main sources of noise contributing to the variance of the cross-sections include Poisson noise and scan noise. However, in this analysis, where the incident electron dose is low, merely around  $600 \text{ e}^-/\text{\AA}^2$ , Poisson noise is the limiting factor on the atom counting reliability.<sup>7</sup> Therefore, the variance on the cross-section of a column with  $g$  atoms equals  $\mu_g/d$ , where  $\mu_g$  represents the mean column-integrated cross-section of columns with  $g$  atoms, and  $d$  the incoming electron dose.<sup>7</sup> Occupancy values for the different Pb sites are calculated by dividing the total number of Pb atoms with the total number of possible Pb positions. The latter is determined by the estimated sample thickness. Since atom counting uncertainties on individual columns are known, the uncertainties on the occupancy values can be readily determined by common error propagation formulas.

## S9 Statistical analysis of Pb clustering

In order to verify whether the distribution of the estimated number of Pb-2 atoms, observed along the viewing directions of SOD cages with similar thicknesses, corresponds to a Poisson distribution, statistical hypothesis testing by using a chi-squared test has been performed at a significance level of 5 %.<sup>8</sup> Hereby, the null hypothesis assumes the observed distribution to be Poisson distributed, whereas the alternative hypothesis assumes the opposite. In Table S3, more details can be found on the hypothesis testing results of Figure 3. The mean  $\lambda$  of the Poisson distributions has been calculated by averaging the number of Pb-2 atoms observed along projected SOD cages with similar thicknesses throughout the sample.

		Projected SOD cage thickness (nm)			
Sample	$\chi^2$ test	16.6-17.8	17.8-19.0	19.0-20.3	20.3-21.5
Pb <sub>1</sub> -LTA	$\chi^2_{\text{calc}}$	104.27	231.46	1412.72	46.07
	$\chi^2_{\text{crit}}$	18.31	16.92	18.31	15.51
Pb <sub>0.5</sub> -LTA	$\chi^2_{\text{calc}}$	27.62	18.11	31.03	38.52
	$\chi^2_{\text{crit}}$	19.68	15.51	16.92	16.92

**Table S3.** Result of verifying by a chi-squared ( $\chi^2$ ) test whether the observed distributions of the number of Pb-2 atoms along the viewing direction of projected SOD cages in the Pb<sub>1</sub>-LTA and Pb<sub>0.5</sub>-LTA zeolite samples follow a Poisson distribution. The statistical hypothesis test has been performed for different SOD cage thicknesses. Hereby, the null hypothesis assumes the distribution to be Poisson distributed. In all cases, the calculated chi-squared values ( $\chi^2_{\text{calc}}$ ) are well above the critical values ( $\chi^2_{\text{crit}}$ ) for a significance level of 5 %, rejecting the null hypothesis.

## References

- 1 W. Baekelant, S. Aghakhani, E. Coutino-Gonzalez, D. Grandjean, K. Kennes, D. Jonckheere, E. Fron, F. D'Acapito, A. Longo, P. Lievens, M. B. J. Roeyfaers and J. Hofkens, *J. Phys. Chem. C*, 2018, **122**, 13953–13961.
- 2 J. Devijver, P. A.; Kittler, *Pattern Recognition: A Statistical Approach*, Prentice-Hall International, UK, 1982.
- 3 S. J. Pennycook, *Annu. Rev. Mater. Sci.*, 1992, **22**, 171–195.
- 4 P. D. Nellist and S. J. Pennycook, 2000, pp. 147–203.
- 5 H. E, K. E. MacArthur, T. J. Pennycook, E. Okunishi, A. J. D'Alfonso, N. R. Lugg, L. J. Allen and P. D. Nellist, *Ultramicroscopy*, 2013, **133**, pp. 109-119.
- 6 G. T. Martinez, A. De Backer, A. Rosenauer, J. Verbeeck and S. Van Aert, *Micron*, 2014, **63**, pp. 57-63.
- 7 S. Van Aert, A. De Backer, L. Jones, G. T. Martinez, A. Béch e and P. D. Nellist, *Phys. Rev. Lett.*, 2019, **122**, 066101.
- 8 P. E. Greenwood and M. S. Nikulin, *A Guide to Chi-Squared Testing*, Wiley, New York, 1996.